

Efficient and recoverable novel pyranothiazol Pd (II), Cu (II) and Fe(III) catalysts in simple synthesis of polyfunctionalized pyrroles: Under mild conditions using ultrasonic irradiation

Mahmoud Abd El Aleem Ali Ali El-Remaily¹  | Nashwa M. El-Metwaly^{2,3}  |
Tahani M. Bawazeer²  | Mohamed E. Khalifa⁴  | Tarek El-Dabea¹  |
Ahmed M. Abu-Dief^{1,5} 

¹Chemistry Department, Faculty of Science, Sohag University, Sohag, Egypt

²Chemistry Department, Faculty of Applied Science, Umm Al-Qura University, Mecca, Saudi Arabia

³Chemistry Department, Faculty of Science, Mansoura University, Mansoura, Egypt

⁴Department of Chemistry, College of Science, Taif University, Taif, Saudi Arabia

⁵Chemistry Department, College of Science, Taibah University, Medina, Saudi Arabia

Correspondence

Prof. Dr. Mahmoud Abd El Aleem Ali El-Remaily, Chemistry Department, Faculty of Science, Sohag University 82524, Sohag, Egypt.

Email: mahmoud_ali@science.sohag.edu.eg; msremaily@yahoo.com

Prof. Dr. Nashwa El-Metwaly, Chemistry Department, Faculty of Applied Science, Umm Al-Qura University, Mecca, Saudi Arabia.

Email: nmmohamed@uqu.edu.sa

Dr. Ahmed M. Abu-Dief, Chemistry Department, College of Science, Taibah University, Medina, P.O. Box 344, Saudi Arabia.

Email: ahmed_benzoic@yahoo.com; amamohammed@taibahu.edu.sa

Funding information

Taif University Researchers Supporting Project, Grant/Award Number: TURSP-2020/43

Abstract

Three novel Pd (II), Cu (II), and Fe (III) complexes were prepared from thiazole ligand through bidentate chelating mode. Alternative spectral and analytical tools were applied to elucidate their structural and molecular formulae. This study was extended to investigate stability and stoichiometry of complexes in solution, using standard methods. In addition, the best atomic distribution within structural forms was obtained by Material Studio Package via the density functional theory (DFT) method. This computational study fed us with significant physical characteristics for differentiation. Also, crystal surface properties in the packing system were studied using the Crystal explorer program, to evaluate the extent of contact between surfaces. Computational data discriminate Pd (II)-thiazole (HYHPd) complex by some physical features, which may be promising in the catalytic field. This complex was selected to play a catalytic function to synthesize polyfunctionalized pyrrole derivatives using ultrasonic irradiation in a one-pot reaction. The catalyst was selected for this application based on the history of Pd (II) complexes and the properties expected theoretically. A condensation reaction for aromatic aldehyde, aromatic amine, acetylacetone, and nitromethane was carried out under mild reaction conditions by ultrasonic irradiation. All reaction conditions were optimized among that variable Lewis acid catalysts in comparison to our new complexes. HYHPd catalyst displayed superiority in overall trials with high yield, short time, and green conditions (solvent H₂O/EtOH). Also, the recovery of hetero-catalyst was succeeded and reused by the same efficiency up to five times after that the efficiency was reduced. The mechanism of action was proposed based on the ability of Pd (II) for adding extra-bonds over z axis and supported by theoretical aspects.

KEYWORDS

benign protocol, DFT studies, HYHPd complex as recoverable catalyst, polyfunctionalizedpyrroles, ultrasonic irradiation

1 | INTRODUCTION

The ultrasonic state increases the rate of organic changes in mild conditions that otherwise require strict pressure and temperature conditions.^[1,2] Ultrasonic irradiation is also used by various synthetic reactions to facilitate the creation, development, and implosive collapse of bubbles in a liquid.^[3] Initiated by cavitation, bubble collapse causes high stresses, extreme local heating, and very short lifetimes. Cavitation acts as a way of focusing the sound's scattered energy.^[4] Ultrasound irradiation can cause several reactions by providing activation energy in contrast to traditional heating that provides thermal energy in the macrosystem.^[5a] Other benefits of ultrasound irradiation include high product yields, low reaction times, minimization of side products,^[5b] and nontoxic and environmentally friendly solvents.^[6]

The reactions between multicomponent reactions (MCRs) facilitate the formation of variable bonds in a one-step process in synthetic chemistry. Also, MCRs are attracting interest as one of the most powerful emerging synthetic tools for creating molecular complexity and diversity, due to their intrinsic atomic economy, selectivity, simplicity, and energy efficiency. Although MCRs have many advantages, it still suffers from several drawbacks as harsh conditions, long reaction time and usage of excessive reagents, and toxic solvents.^[7,8]

Pyrrrole-based structure has achieved significance in heterocyclic chemistry, due to its numerous applications.^[9] Polysubstituted pyrroles play an important role as synthetic intermediates, pharmacophores, and functional materials of these respective groups of compounds.^[10] Variable standard methods were approved for polysubstituted pyrrole synthesis.^[11] Although several processes have been reported previously, functionalized pyrrole synthesis is a challenging task for researchers worldwide. This is due to a lack of selectivity and polymerization issues.^[12] The most proper method used to prepare polysubstituted pyrroles via reaction of phenyliodonium ylides and enamine esters using $\text{BF}_3 \cdot \text{Et}_2\text{O}$ was demonstrated.^[13] A simple oxidative cyclization method for β -enamine ketones, esters, and alkynoates using CuI in addition to oxygen was reported.^[14] Under mild conditions, AgOAc regulated one-pot condensation approach was used to acquire pyrroles (3,4-disubstituted) from accessible aldehydes and amines.^[15] $\text{Cu}(\text{NTf}_2)_2$ was used as a catalyst to synthesize regioisomeric polysubstituted N-H pyrroles from 1,3-dicarbonyl compounds.^[16] 3,4-diaryl-(1H)-pyrroles were synthesized from aryl alkenes and tosylmethylisocyanide.^[17] Zinc (II) chloride was utilized to synthesize substituted pyrroles and through regioselective propargylation/amination/cyclo isomerization as a multifunctional catalyst.^[18] Via intermolecular

addition of oximes to activated alkynes and subsequent thermal rearrangement of O-vinyl oximes through nucleophilic catalysis, a descriptive synthesis of highly substituted pyrroles was also recorded.^[19] An effective method for synthesis of polysubstituted pyrroles by 4C and 1N-cyclization of 4-acetylene ketones with primary amines using FeCl_3 was identified. As a heterogeneous catalyst, substituted pyrroles have recently been synthesized using iron-containing metal-organic frameworks (MOFs).^[20a] Synthesis of polysubstituted pyrroles by β -cyclodextrin as an effective and recoverable supermolecular catalyst in aqueous medium was performed.^[20b]

Accordingly, polysubstituted pyrrole derivatives catalyzed by palladium (II) complexes by ultrasonic irradiation under mild conditions have not been reported. Proceeding from these studies, we aimed synthesis and characterization for series of Cu (II)-, Fe (III)-, and Pd (II)-thiazole complexes. This targeted to develop a new route about the catalytic role of palladium (II) complex in synthesizing bio-active heterocyclic compounds by multicomponent reactions. With merits of environmentally benign, readily accessibility, cost-benefit and according to historical catalytic uses of Pd (II) complexes, Pd (II)-thiazole complex (HYHPd) may be promising reusable catalyst in a facile one-pot synthesis. Such to synthesize hybrid molecules polysubstituted pyrroles **5a-o** through coupling reaction of aromatic aldehyde, aromatic amine, acetylacetone and nitromethane using ultrasonic irradiation under mild conditions. All products have been deposited in excellent yields after a short reaction time. Computerized studies around new complexes to illustrate physical properties of HYHPd complex, which pushed for its catalytic use.

2 | EXPERIMENTAL

2.1 | Synthesis of thiazole derivative (HYH)

The ligand is prepared according to the procedures mentioned in Abu-Dief et al.^[21] as follows: a mixture of 2, 4-thiazolidinedione (10 mmol), arylidenemalononitrile (10 mmol), and piperidine (20 mmol) in 20-ml ethanol was heated under reflux for 2 h at 200°C. Arylidenemalononitriles were prepared according to the known procedure. The mixture was tested by Thin layer chromatography (TLC) to check the complete conversion for starting materials. A yellow precipitate of 2-amino-6-oxo-3-(piperidinylamidino)-4-(4chlorophenyl)-6,7-dihydro-pyrano[2,3-d]-5,7 thiazol was filtered off, washed by ethanol and dried. Its empirical formula was

$C_{18}H_{19}N_4O_2SCl$; m.p. 230°C; solubility: ethanol; molecular weight: 390.5 (Table S1).

Notice that HYH was the ligand abbreviation used in this article for simplicity, which derived from the second letters in the ligand main component (thiazol-pyrano-chlorobenzaldehyde).

2.2 | Synthesis of metal complexes

The investigated complexes were synthesized according to the procedures mentioned in Abu-Dief et al.^[21] as follows: HYH ligand (5 mmol) was mixed with 5 mmol from each of the following salts: $[Cu(OAc)_2]H_2O$ and $[Fe(NO_3)_3] \cdot 9H_2O$ in hot ethanol (10 ml), while $[Pd(OAc)_2]$ in hot acetone (10 ml). Then each mixture was heated under reflux for 2–3 h at 90°C. The precipitated complexes were filtered and washed with hot ethanol or acetone, as shown in Scheme 1.

2.3 | TGA and kinetic and thermodynamic parameters

This study aims to examine the thermal stability of complexes under constant heating rate and then derived thermo-kinetic parameters by using the Coats–Redfern equation.^[21,22] By which, a fraction decomposes (α) at time t , which considered a temperature-dependent function was applied in this relation; $da/dt = k(T)f(\alpha)$, where $f(\alpha)$ is a function for conversion, $k(T)$ is Arrhenius type ($k = Ae^{-E^*/RT}$), and R is gas constant. The two equations were interpreted to estimate this relation, $da/dt = (A/\varphi e^{-E^*/RT})f(\alpha)$ and φ is a linear heating rate (dT/dt). Consequently, integration followed by approximation, $\ln(\alpha) = -[E^*/RT] + \ln[AR/\varphi E^*]$ was achieved, where, $g(\alpha)$ is based on the mechanism of reaction and the right side (integral) is temperature dependent. So the kinetic parameters (A and E^*) can be calculated according to the following equation.

$$\ln \left[-\frac{\ln(1-\alpha)}{T^2} \right] = -\frac{E^*}{RT} + \ln \left[\frac{AR}{\varphi E^*} \right].$$

From the relation between left side and $1/T$ the activation energy (E^*) and pre-exponential factor (A , s^{-1}) can be obtained from the slope and intercept, respectively. Therefore and by using kinetic parameters, thermodynamic parameters (ΔS^* , ΔH^* , and ΔG^*) can be calculated by simple relations.^[21,23,24]

2.4 | Formation constants for stoichiometric complexes in solution

Stoichiometry of complexes prepared in solution state was characterized by using Job's and mole ratio

methods,^[21,24–26] which may agree with that in the solid state. The measured absorbance was plotted versus mole fraction of ligand or mole fraction of metal ions. Then the formation constants (K_f) were calculated using the continuous variation method (Job's). The molar ratio of complexes formed in solution was obtained from the following equation^[27]:

$$K_f = \frac{A/A_m}{(1 - A/A_m)^2 C},$$

where A_m is the maximum absorption at the stabilized ratio of complex, C is the molar concentration of metal, and A is the absorbance values at either part on absorbance peak. Also, the changes in free energy (ΔG^*) of complexes were estimated from this relation; $\Delta G = -RT \ln K_f$, where R is the gas constant at 25°C and T is the temperature (kelvin).

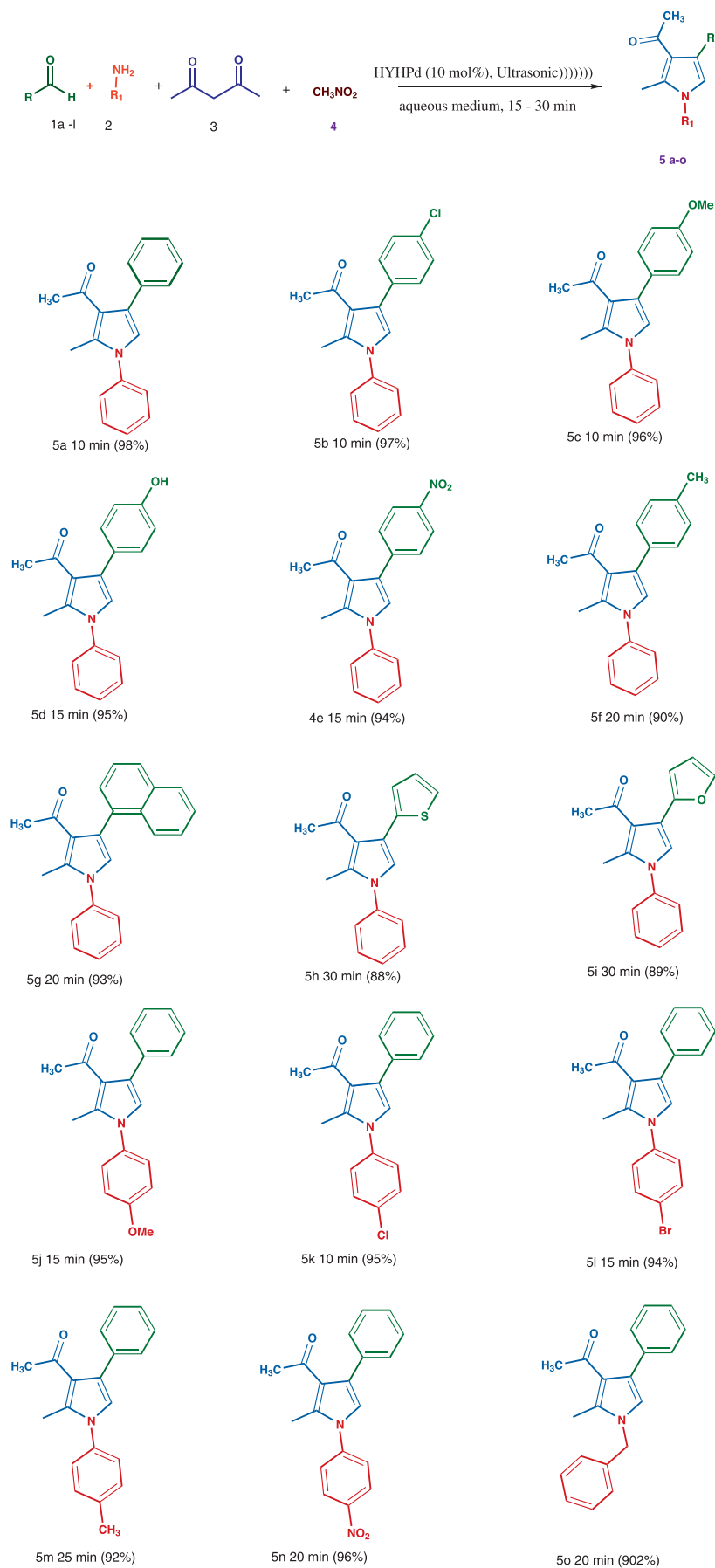
2.5 | Heterogeneous catalytic synthesis for polysubstituted pyrroles 5a–o

In a round bottom flask, HYHPd complex (10 mol%) was mixed with 30 ml (v/v) of H_2O /ethanol (3/1) at 25°C using a magnetic stirrer. Then aromatic aldehyde **1** (1 mmol), aromatic amine **2** (1.5 mmol), acetylacetone **3** (1 mmol), and nitromethane **4** (1 mmol) were added. At 20-kHz frequency and 40-W powers at 60°C, the sound was applied and sounded for the desired acceptable time (Scheme 2), and then the purity of the product was tested by TLC. Each reaction mixture was allowed to cool till 25°C and then isolate the catalyst by filtration. Organic materials were extracted by ethyl acetate (3×10 ml), the polysubstituted pyrroles derivatives **5a–o** that combined organic phases, were washed by water, and after that were dried over anhydrous Na_2SO_4 then concentrated under reduced pressure. The resulting solid product was filtered and recrystallized from 5-ml ethanol to give a pure product, which characterized by M. P, Fourier transform infrared (FT-IR) and nuclear magnetic resonance (NMR) spectra (the techniques were typed in the supporting information).

2.6 | Catalyst recovery and reuse

Heterogeneous catalyst (HYHPd) could be easily reused many times after its separation by filtration at the end of each catalytic usage. The filtered catalyst must be washed by ethanol and bi-distilled water after that dried at 90°C for 3 h. According to the re-cyclic feature of catalyst, it can be used for another reaction under typical conditions.

SCHEME 2 Polysubstituted pyrrole derivatives **5a–o**, time of reaction (min) and yield (%)



2.7 | Optimization procedure

Materials Studio package^[28a] was one of the most advanced programs that has a good reputation in geometry optimization credibility.^[28b-d] Atomic building and maps of HYH ligand and its complexes were extracted by using DMOL3 program under density functional theory (DFT) method, which regulated at double numerical plus polarization (DNP) basis set.^[29] The exchange-correlation function was selected upon generalized gradient approximations (GGA) and revised Perdew–Burke–Ernzerh (RPBE) functions.^[30] Also, Fukui indices were estimated under DFT-semi-core pseudopods values (dspp) with polarization functional (DNP) and double numerical basis sets, as the optimum conditions.^[31]

3 | RESULTS AND DISCUSSION

3.1 | Preliminary properties

Molecular formulae of the ligand and its complexes were proposed first according to elemental analyses and molar conductivity. The molar ratio suggested for Fe (III), Pd (II), or Cu (II) complex was 1M:1L. Also, the molar conductivity was measured for all complexes, and they appeared to have nonconducting or non-electrolytic property.^[27c] This may refer to the high-covalent nature of conjugated anions found in metal salts (Table S1).

3.2 | IR, ¹H, and ¹³C NMR spectra

The nature of bonding between HYH ligand and metal ions was evaluated from these spectral techniques starting with IR-spectral data (Figure S1). By comparing the HYH spectrum with that of its complexes, ν (NH) vibration suffers shift from 3401 to 3415, 3428, and 3434 cm^{-1} in HYHFe, HYHPd, and HYHCu spectra, respectively. Also, ν_{as} (NH₂) and ν_{s} (NH₂) vibrations in complexes spectra were appeared shifted from 3311 and 3220 cm^{-1} to bands that seem overlapped with ν (NH) and ν (OH) vibrations. The broadness in high-frequency region due to the presence of water molecules prohibits exact discrimination between these vibrations.

The overall changes in ν (NH) and ν (NH₂) vibrations denote their coordination with metal ions, which mainly happened after destroying intraligand H bonding.^[32] Also, acetate vibrations [ν_{as} (OAc) and ν_{s} (OAc)] in HYHCu and HYHPd were observed at 1450; 1290 cm^{-1} and 1433; 1251 cm^{-1} , respectively. Whereas and sequentially, ν_{as} (NO₃) and ν_{s} (NO₃) were observed at 1520 and 1350 cm^{-1} . The separation between two bands

($\Delta = \nu_{\text{as}} - \nu_{\text{s}}$) points to the coordination of two anions as monodentate ligands. Extreme shift of ν (C=O) vibration to high wavenumber is evidence for its siding from coordination. ν (M–N) and ν (M–O) bands were also recorded at low wavenumber region.^[24,33,34] All essential vibrations were tabulated (Table S1).

Identity of HYH and HYHPd agrees with NMR spectroscopic analysis (Table 1), so the obtained figures and extracted data were displayed for explanation (Figures S2–S4 and Table 1). The downfield shift of NH₂ and NH signals in HYHPd spectrum indicates their coordination. Multiplet signals appeared at δ (ppm) = 1.46–1.51 were assigned for protons of 2(CH₃) in acetate groups and 3CH₂ of piperidine ring. The other signals of 2CH₂ group of the piperidine ring lie below signals of solvent (DMSO and its water). Furthermore, ¹³C NMR spectrum of HYH (Figure S2) exhibited the following signals (ppm), 170.96 for (C=O), 162.42 for (N–C = NH), 129.41, 129.16 for aromatic carbon atoms (4CH–Ar), 24.19–45.66 range for aliphatic carbon atoms (5 CH₂–Aliph).

3.3 | Electronic spectra, magnetic susceptibility, and optical band gap measurements

Ultraviolet–visible (UV–Vis) spectra of new complexes were obtained (Figure S5), to extract effective transition bands that coincided with strict geometry (Table S2). Each spectrum was performed in DMF solvent under irradiation from 200- to 800-nm range at 25°C. Significant transitions and quantitative molar absorptivity (ϵ_{max}) were aggregated in Table S2. With respect to free ligand spectrum, the intraligand transitions have appeared at 296, 360, and 392 nm which attribute to $n \rightarrow \sigma^*$, $\pi \rightarrow \pi^*$, and $n \rightarrow \pi^*$, respectively. An observable shift of $n \rightarrow \pi^*$ band has appeared clearly in all complexes than that in the HYH spectrum. This appearance indicates changes upon lone pair of electrons over donor atoms that

TABLE 1 ¹H NMR of the synthesized HYH ligand and HYHPd complex

Compounds	¹ H NMR(δ , ppm) in DMSO-d ₆
HYH	9.88 (s, 1H, NH), 7.45–7.42 (d, 2H, ArH), 7.34–7.32 (d, 2H, ArH), 7.04 (d, 2H, NH ₂), 4.63 (d, 1H, CH), 4.44 (d, 1H, C=NH), 3.34–3.20 (t, 4H, 2CH ₂), 1.56–1.47 (m, 6H, 3CH ₂)
HYHPd	9.96 (s, 1H, NH), 7.8–7.4 (d, 2H, ArH), 7.37–7.2 (d, 2H, ArH), 6.94 (d, 2H, NH ₂), 4.63 (d, 1H, CH), 4.44 (d, 1H, C=NH), 1.54–1.46 (m, 12H, 3CH ₂ and 2CH ₃ of acetate groups)

Abbreviation: NMR, nuclear magnetic resonance.

coordinated. Also, important d–d transitions were summarized, and their attributes were appeared (Table S2). Accordingly, octahedral geometry was proposed for HYHCu and HYHFe, while a square planer was proposed for HYHPd.^[35] Moreover, the degree of ligation and type of new bonds within HYHFe can be known after calculating 10Dq, Racah(B), and nephelauxetic (β), as the ligand field parameters. The values were 8598.8 cm⁻¹, 781.7, and 0.77, respectively, and appeared to match with octahedral geometry that having ionic characteristics for new Fe–L bonds.^[24,36]

Furthermore, the magnetic moment (μ_{eff}) of the titled chelates (Table S2) was calculated to confirm the structural formula proposed. The value estimated for the HYHCu complex (1.73) closes to spin-only moment for d⁹ systems,^[26a] while the value calculated for HYHFe complex ($\mu_{\text{eff}} = 5.43$ B.M.) assigns to high spin octahedral geometry.^[37] The diamagnetism of the HYHPd complex was expected with its square planar geometry for dsp² hybridization.^[26a]

The optical band gap (E_g), which is known by the separation between the ground and excited states, can be estimated from UV–Vis spectra. So E_g value was the lowest $h\nu$ required to release electron completely from its positive hole, although the attraction force in between. The lower the band gap value, the ease of excitation and the conduction band will be close to the optical one. This feature reflects some specific properties that depend on electron fluent over the compound as, activation energy and semiconductors like.^[38a,b] As known, the lower activation energy required the success of catalytic behavior of such complex. Also, the energy level of Cu 3d > Fe 3d > Pd 4d orbitals has an impact on activation energy as well as the catalytic behavior. E_g values can be calculated from the following relations^[38]:

$$\alpha = 1/d \ln A \quad (1)$$

where d is the width of the cell.

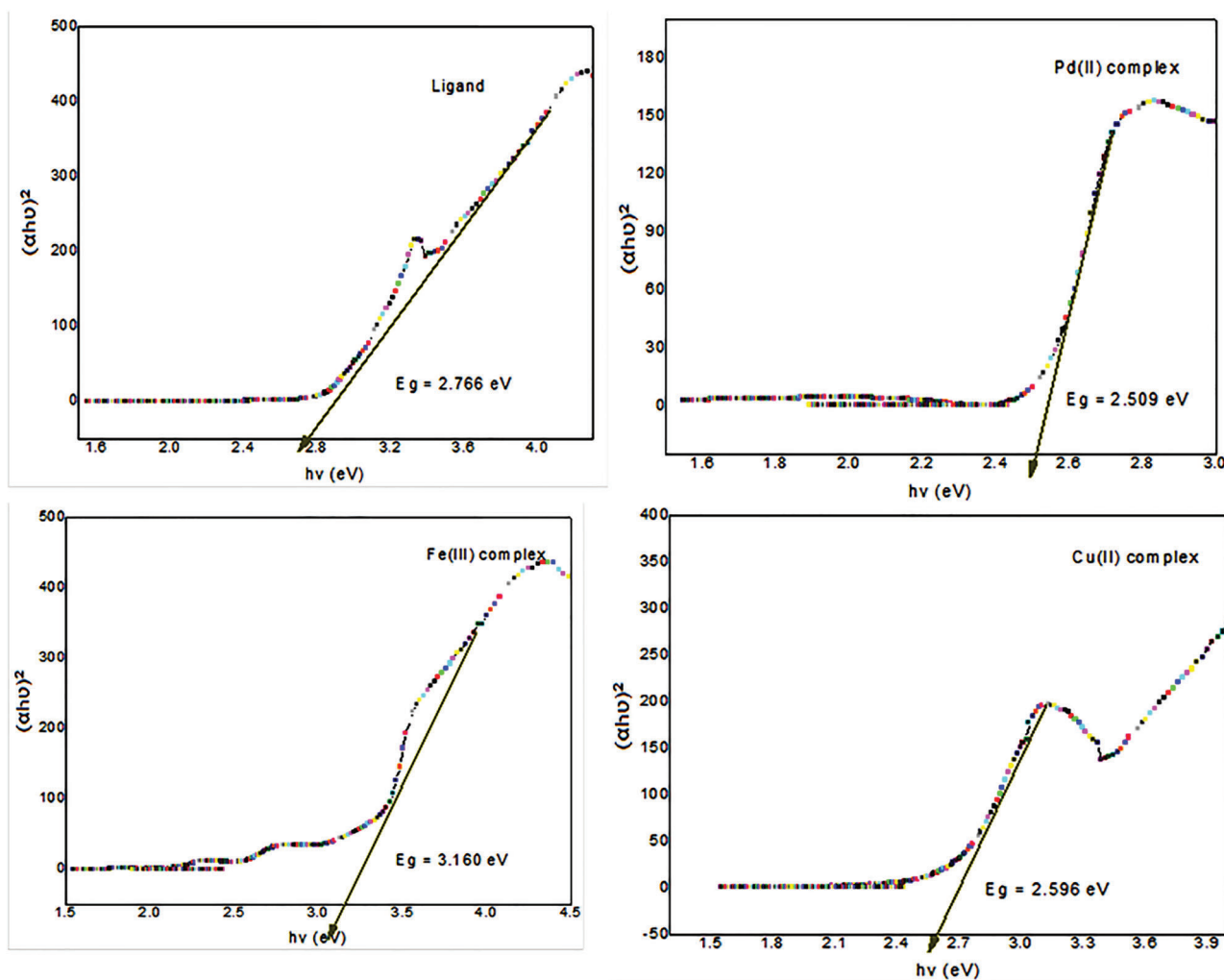


FIGURE 1 Optical band gap plots for HYH ligand and its complexes

$$\alpha h\nu = A(h\nu - E_g)^m \quad (2)$$

where α is absorption coefficient and A is energy-independent constant.

Where m is 0.5 or 2 for direct or indirect transition, respectively, then the values of α can be calculated (relation 1) and used to calculate $(\alpha h\nu)^2$, which conducts to draw relation versus $h\nu$ (Figure 1). A leaner relation was drawn and from extrapolating line with the x axis at $(\alpha h\nu)^2 = 0$, E_g value can be estimated. It is worthy to mention that, low optical band gap value (2.509 eV) was recorded with HYHPd complex. This predicts promising applications when utilizing HYHPd complex either in a solar cell or in catalytic usage, as already done in this study.^[39]

3.4 | Thermogravimetric and kinetic studies

Thermogravimetric analysis (TGA) aims to evaluate the thermal stability of three complexes under consideration, and the plausible degradation behavior was estimated (Scheme S1 and Table 2). These data tooled up if H₂O molecules in a crystal lattice or inside coordination sphere. The features of TGA steps indicate reduced thermal stability of all complexes and the residual parts reflect the mononuclear presence in all of them.^[40] Thermo-kinetic parameters of fused complexes were valued for degradation steps and recorded (Table 2). Sequenced decomposition steps displayed a gradual increase in positive Gibbs free energy (ΔG^*) values, which means faster formation reaction than the degradation reaction with in the non-spontaneous process. Also, negative entropy (ΔS^*) values reflect that the activated complex is further orderly than initial reactants,^[41,42] while positive ΔH^* values coincide with endothermic degradation steps. A relation between E^* and A displayed, low value of a , which suggests a slow degradation reaction, whereas high positive values of E^* confirm that the processes involved rotational, translational, and vibrational states in addition to changes of energy are mechanical potential.^[24,43]

3.5 | Complexes stoichiometry in solution

3.5.1 | Continuous variation and molar ratio methods

Continuous variations and molar ratio routes evaluate stoichiometry of synthesized complexes after their

development in solution through the direct reaction between HYH and each metal salt (Cu (II), Pd (II), or Fe (III)). Curves of the continuous-variation method (Figure S6) showed the maximal absorbance at a mole fraction of X-ligand = 0.5, in accordance to 1M:1L molar ratio. The formation constants (K_f) were estimated,^[27] and the order of values is as follows: HYHPd > HYHCu > HYHFe. Although this arrangement belongs to complexes in the solution state, it may agree with their solid state. The formation process is spontaneous based on negative Gibbs free energy values.^[24,44] Also, molar ratio curves for the formed complexes (Figure S7) exhibited the same ratio proposed (1M:1L) with solid state.

3.5.2 | Impact of pH on complexes stability

The impact of acidity of the medium on complexes stability is known, and its evaluation has an effective influence on complexes usage in different application fields. The obtained profiles showed typically separated curves under variable pH_s (Figure S8), and the steady range has appeared at pH = 4–10. Such a wide range of stability reflects the safe use of such complexes in broad pH range during different applications, as catalysis aimed.

3.6 | Conformational analysis

This computational study was executed by Materials Studio package under DMOL3 module with DFT method (DNO basis set). This study adds a further assertion on binding mode and exports essential physical properties, to recognize features of new synthesizes.

HYH ligand structure (Figure S9) clarifies the *cis*-orientation of NH and NH₂ groups, which lets their coordination with one central atom, as spectrally suggested. The structural forms of complexes (Figure S9) appeared without any unfavorable strain in bonds, which reflects their normality. Frontier orbitals (Figure 2) reveal focusing of highest occupied molecular orbital (HOMO) around thiazole moiety in the free ligand, while lowest unoccupied molecular orbital (LUMO) appeared to cover the whole HYH structure. On the other side and with respect to complexes, the two levels appeared extended over the molecules. This points to the presence of excess labile electrons in complexes, which leads to electronic transitions under a lower activation energy. This conclusion is strictly supported by lower energy gap between the two levels in three complexes than the free ligand. Other characteristics were taken as atomic charges, bond lengths, Fukui indices, local softness, local

TABLE 2 Plausible thermal decomposition for tested complexes as well as kinetic and thermodynamic parameters

Complexes	Temperature (°C)	Fragment loss (%)		M. Wt.	Lost form	E^* (kJ mol ⁻¹)	A (S ⁻¹)	ΔH^* (kJ mol ⁻¹)	ΔG^* (kJ mol ⁻¹)	ΔS^* (J mol ⁻¹ K ⁻¹)
		Found	Calc.							
HYHCu	35–120°C		H ₂ O	18		43.79101	1.85	43.15	63.43	-263.427
	122–307°C		C ₄ H ₁₀ O ₆	154		(2.87)		42.01	100.20	-271.927
	309–478°C		C ₁₂ H ₁₅ N ₂ Cl	222.5		(35.54)		40.52	149.37	-276.981
Residue	480–685°C		C ₆ H ₄ N ₂ SO	152.07		(24.29)		38.95	202.05	-280.246
	>685°C		CuO	79.55		(12.71)				
HYHFe	35–110°C		0.5H ₂ O	9		10.90	1.39	10.31	30.08	-274.664
	112–350°C		(NO ₃) ₃ + H ₂ O	204		(1.36)		8.98	74.67	-284.358
	352–490°C		C ₁₂ H ₁₅ N ₂ Cl	222.5		(33.72)		7.40	129.22	-289.349
Residue	492–690°C		C ₆ H ₄ N ₂ SO	152.07		(23.04)		5.99	178.66	-292.169
	>690°C		0.5Fe ₂ O ₃	79.8		(11.94)				
HYHPd	35–110°C		2H ₂ O	36		78.213	0.094	77.606	96.47	-258.471
	112–310°C		C ₄ H ₆ O ₄	118		(5.53)		76.46	132.86	-267.297
	312–450°C		C ₁₂ H ₁₅ N ₂ Cl	222.5		(34.18)		75.046	178.76	-272.211
Residue	452–700°C		C ₆ H ₄ N ₂ SO	152.07		(23.36)		73.42	232.19	-275.648
	>700°C		PdO	122.4		(18.8)				

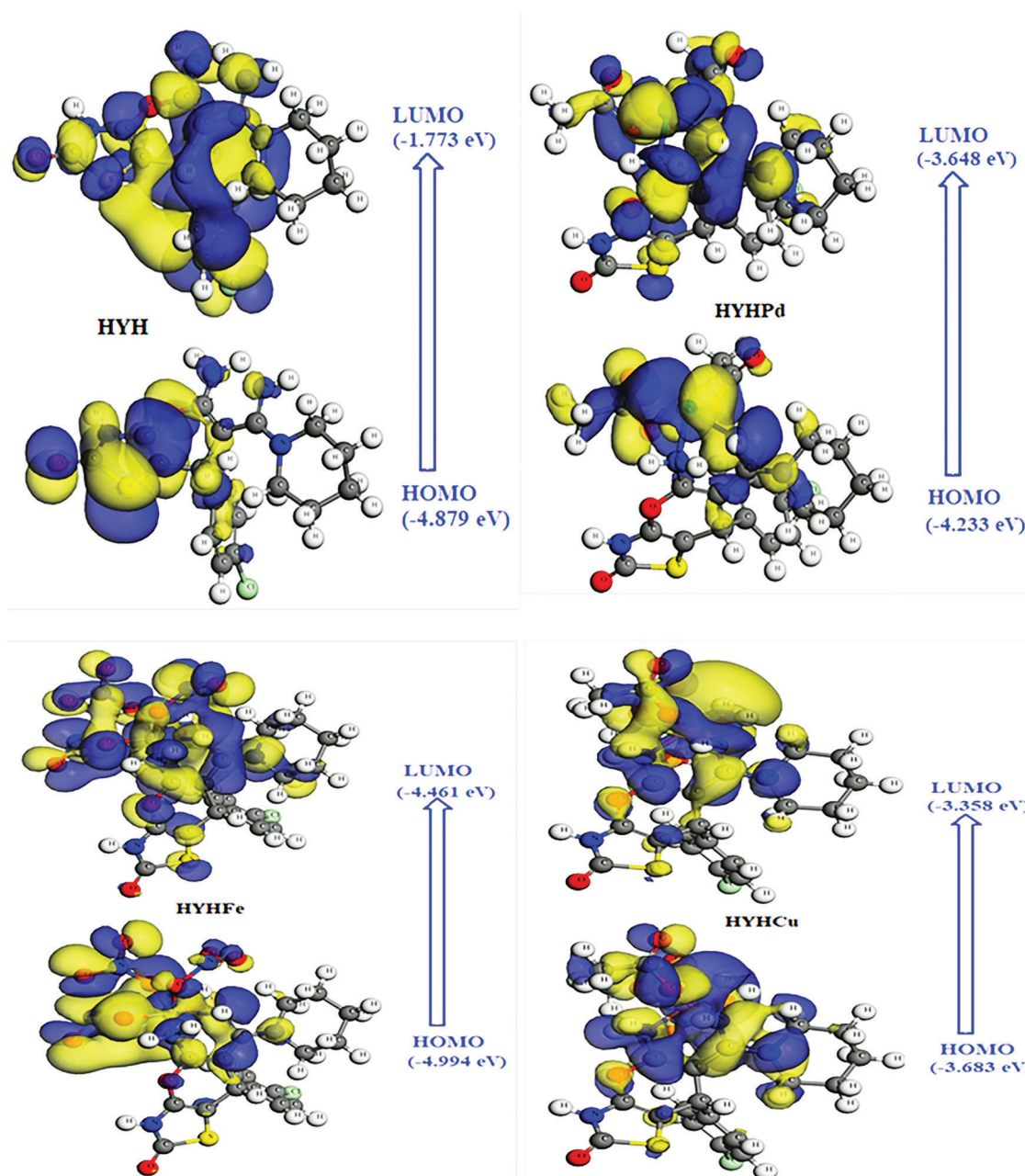


FIGURE 2 Highest occupied molecular orbital (HOMO) and lowest unoccupied molecular orbital (LUMO) images of HYH ligand and its complexes

electrophilicity, and molecular electrostatic maps (MEPs), to put a good view about some significances.

3.6.1 | General features

1. Charges on N(18) and N(19) atoms were appeared by high negativity enough for their coordination and after complexation, and such charges were improved due to $M \rightarrow L$ charge transfer (CT) (Figure 3).
2. Bond lengths of C(4)–N(19) and C(17)–N(18) suffer elongation in three complexes, due to coordinate

bonds formed from these nitrogen atoms. The coordinate bond weakens and elongates other adjacent bonds as C(4)–N(19) and C(17)–N(18) (Table S3).^[45]

3.6.2 | Electrostatic maps and global reactivity

MEP maps were demonstrated for HYH ligand and its complexes to discriminate nucleophilic, electrophilic, and zero potential regions (Figure 4). Such regions were

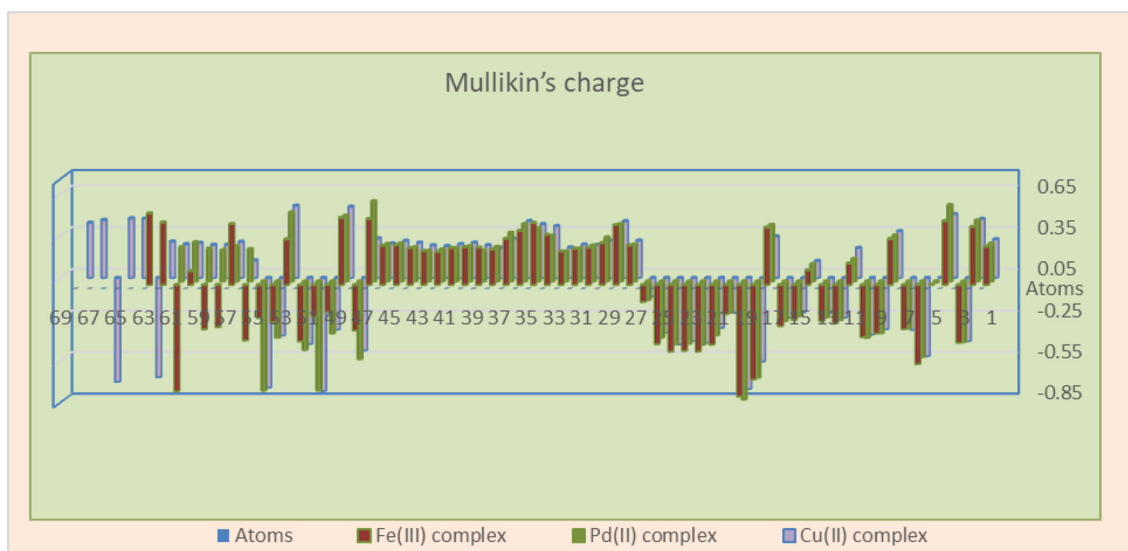


FIGURE 3 Mulliken's charges of HYH and its complexes

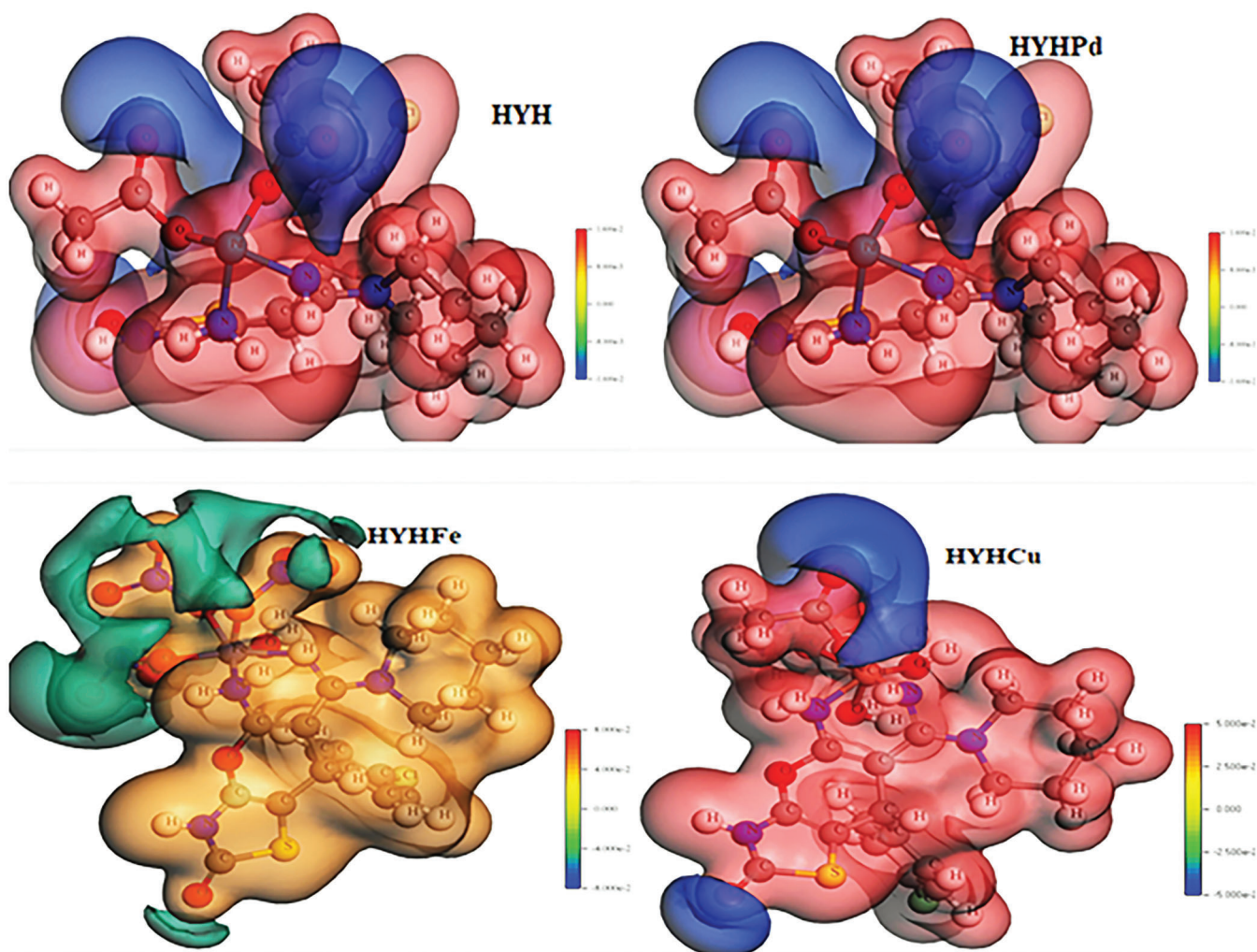


FIGURE 4 Molecular electrostatic maps (MEPs) of HYH ligand and its complexes

depicted by red, blue, and green colors, respectively.^[46] The nucleophilic feature was prevailing on the ligand and its complexes except HYHFe one. Moderate electrostatic potential appeared in the HYHFe complex map, clearly. This feature may refer to the presence of electron-rich acetate anions as a secondary ligand in HYHCu and HYHPd complexes, while HYHFe contains electron-withdrawing nitrate groups.

Fukui indices were obtained from DMol3 module under double numerical polarization (DNP) basis set. Using such indices, local softness (S^- , S^+ , and S^0) and local electrophilicity (W^- , W^+ , and W^0), were calculated by known equations.^[47] Nucleophilic (f_k^+), radical (f_k^0), and electrophilic (f_k^-) attack were estimated (Tables S4–S7). The high nucleophilic (f_k^+) attacks maybe happened on N(18) and N(19) sites (Table S4), which loss their feature after complexation but mostly reversed

(Tables S5–S7). Also, high electrophilic (f_k^-) attach maybe happened on metal centers. Furthermore, the overall local softness (S^- , S^+ , and S^0) and local electrophilicity (W^- , W^+ , and W^0) were estimated and also displayed. Softness values over most atoms in ligand or complexes predict prevailing the softness feature, which is preferable in many applications, while electrophilicity indices appeared significant in the HYHFe complex and reflect a shortage in electron density over the whole molecule.^[48]

3.7 | Crystal packing features

Hirshfeld implemented Crystal explorer software 3.1,^[49] to demonstrate the default crystal shape of the tested complexes. The structural forms must be oriented firstly over VESTA package screen.^[50] Three-dimensional

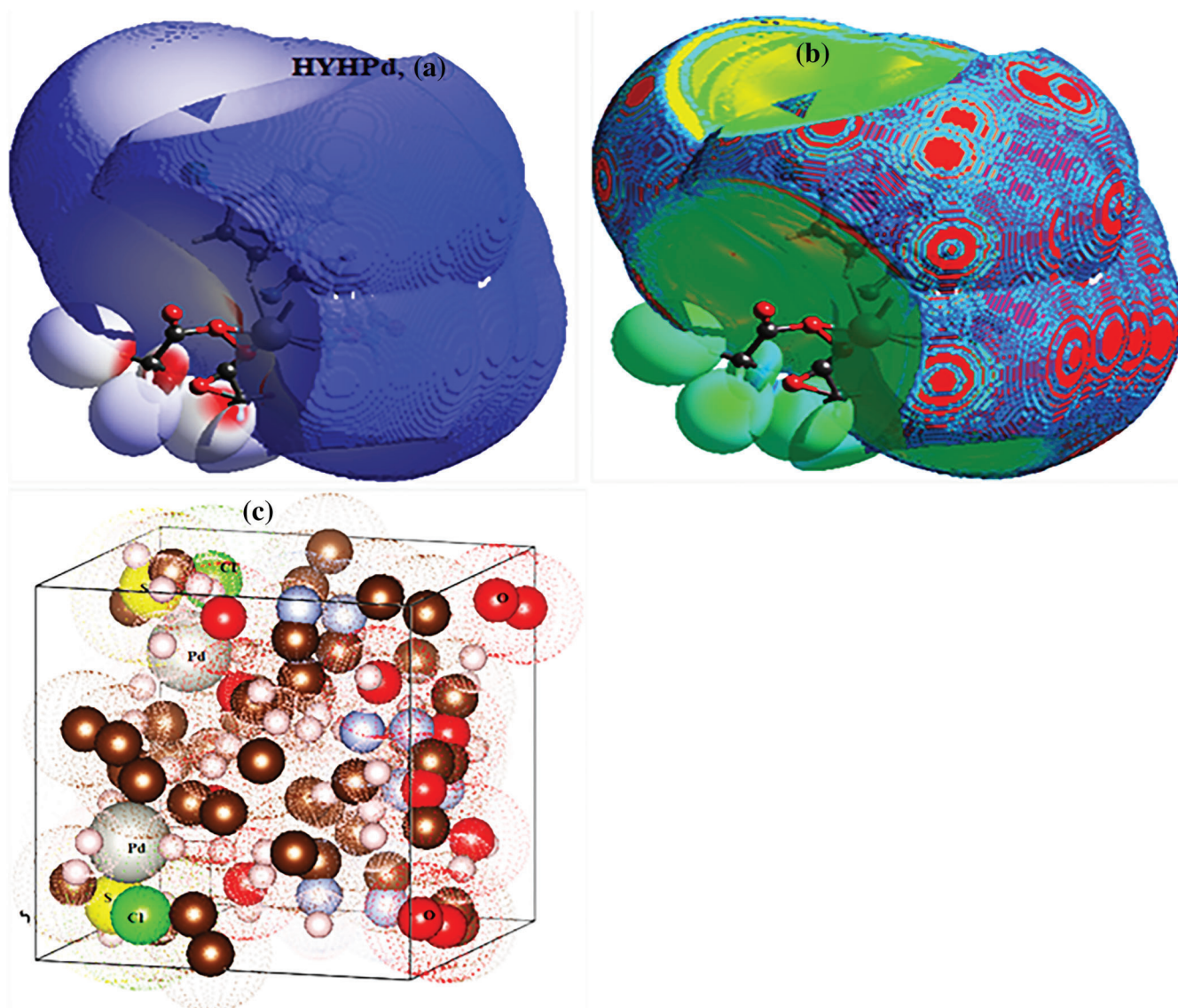


FIGURE 5 Crystal models of d norm (a), curvedness (b), and unit cell of HYHPd complex (c)

models of the complexes were performed by normalized contact distance (d_{norm}) and curvedness styles (Figures 5 and S10). The d_{norm} model, differentiates the magnitude of contact between neighboring crystals inside the packing system. This was clarified by different colors as red, white, and blue as indicators for strong, moderate, and weak contacts, respectively. The strength of contact

between molecular surfaces is attached strongly with the distance in between. The shorter the distance, the stronger the contact, in agreement with van der Waals radii. H bonding is the main route of contact between surfaces. Red spots have appeared around conjugated anions, which considered the suitable contact center. Also, a curvedness style was performed to display surface patches, which suitable for many contact spots in addition to the main contact site (anion).^[51] A moderate contact feature can be expected for all complexes in their crystal packing systems.

The unit cell of HYHPd complex was demonstrated on VESTA screen and appeared closer to body-centered cubic. This appearance displayed Pd centers with farther distribution in crystal, which may serve well in catalytic application. Also, crystal surface properties (Table 3) discriminate HYHPd by its high volume, surface area,

TABLE 3 Hirshfeld crystal packing properties for HYH-complexes

Properties	HYHFe	HYHPd	HYHCu
Volume (\AA^3)	2513.78	2811.78	2141.24
Area (\AA^2)	1260.12	1356.45	1151.60
Globularity	0.710	0.710	0.698
Asphericity	0.044	0.005	0.038

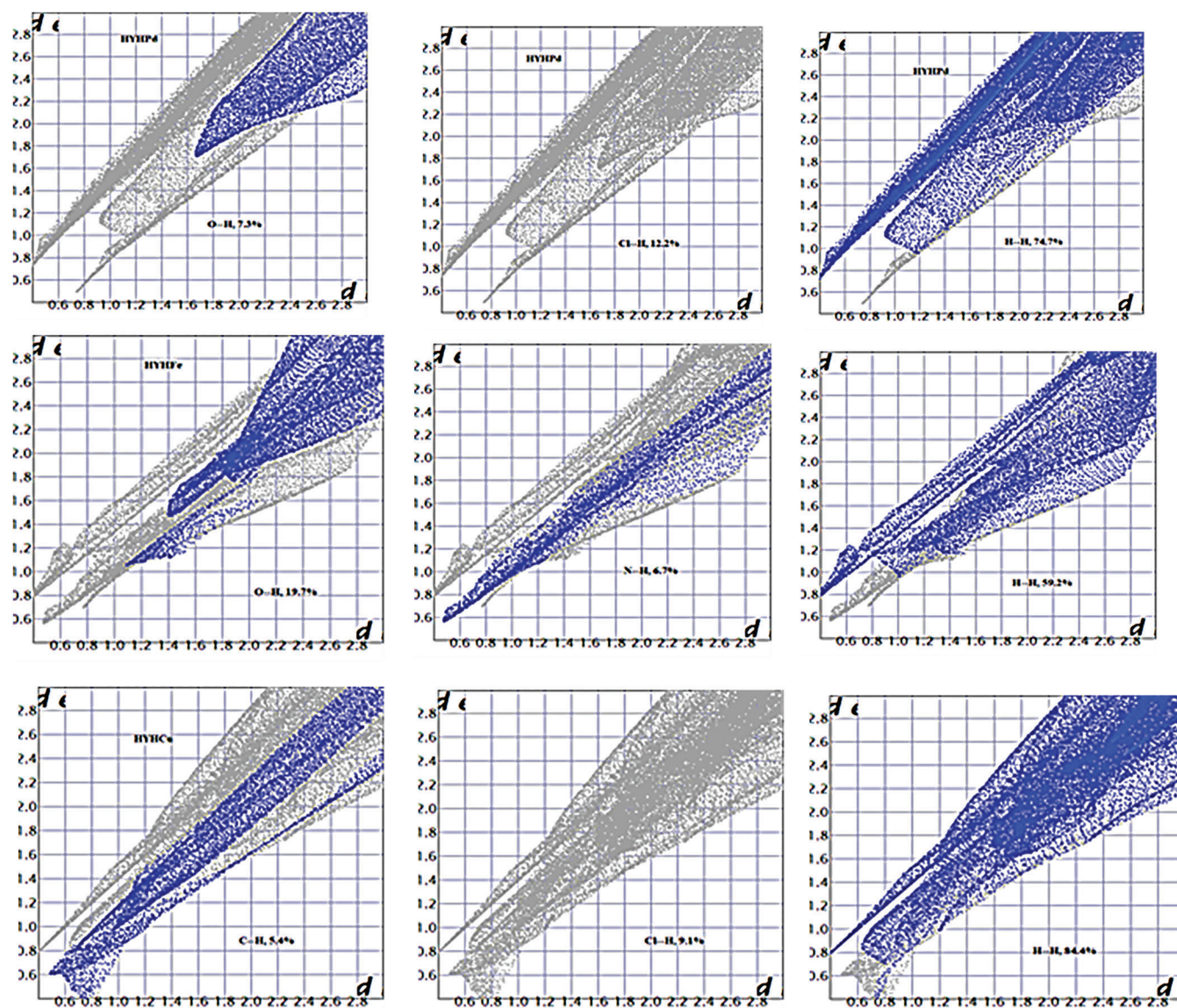


FIGURE 6 Two-dimensional fingerprint plots of HYH complexes

globularity, and reduced asphericity. Furthermore, 2-D fingerprint plots were established to clarify elemental contribution in surface contact (Figure 6). Accordingly, the elemental contribution in HYHPd complex was O–H (7.3%), Cl–H (12.2%), and H–H (74.7%), while the elemental contribution in the HYHFe complex was O–H (19.7%), N–H (6.7%), and H–H (59.2%). The effective contribution was recorded from O and H atoms as preferable contact sites between crystal surfaces.^[52]

3.8 | Hetero-catalytic approach to synthesize polysubstituted pyrrole derivatives 5a–o

HYHPd was selected to play such a catalytic role based on its history as well as its promising characteristics illustrated formerly. The aim is the use of HYHPd to synthesize bioactive polysubstituted pyrroles under heterogeneous catalysis with ultrasonic irradiation conditions. In this context, facile one-pot and four-component condensation reaction as aromatic aldehyde **1** (1 mmol), aromatic amine **2** (1.5 mmol), acetylacetone **3** (1 mmol), and nitromethane **4** (1 mmol) by ultrasonic irradiation were designated as a model reaction. Through the present experiments, proceeded condensation reaction has systemically studied the influence of catalytic dose, reaction-solvent and different Lewis acid or Lewis basic catalysts, on catalytic activity. The product was obtained at a longer reaction time without catalyst and ultrasonic irradiation, while ultrasonic irradiation was only used without a catalyst; the product was more efficient at a longer reaction time. But there was improved yield in presence of HYHPd catalyst and ultrasonic irradiation environment, which appeared excellent after a short reaction period. In presence of HYHPd and ultrasonic irradiation environment, sequences of aromatic aldehydes that undergo electrophilic replacement reactions, were successfully synthesized (as clarified in Scheme 2).

3.8.1 | Effect of catalyst loading

The relationship between catalyst dosages and the product yields was shown in Table 4. In particular, loading of

Entry	Cat. (mol%)	Yield (%) ^a	Entry	Cat. (mol%)	Yield (%) ^a
1	3	18	5	8	83
2	5	40	6	9	92
3	6	56	7	10	98
4	7	74	8	11	98

^aIsolated yields based on **5a**, **1a** (1 mmol), **2** (1.5 mmol), **3** (1 mmol), and **4** (1 mmol) in mixture of water and ethanol (3:1 ratio) by ultrasonic irradiation condition, 10 min.

catalyst from 3 to 10 mol% improved product yield from 18% to 98% (Table 4). The increasing amount of HYHPd improves product yield, which may refer to the increasing number of available active sites. This will lead to brooded catalyst surface that directly contact with four reactants and facilitates their collision to start the reaction. Notably, the further increase of loaded catalyst from 10 to 11 mol% did not affect significantly the yield or reaction time (Table 4). Thus, 10 mol % of catalyst is the optimal amount needed from the catalyst.

3.8.2 | Effect of solvents

To demonstrate the effective procedure, we must detect the effect of several known solvents that were chosen as a medium, for comparison (Table 5). The role of the solvents was evaluated with the model reaction **5a** (i.e.). As indicated in Table 6, the polar protic solvents (MeOH, EtOH, AcOH, and H₂O) were much better than aprotic solvents (DCM, DMF, THF, CH₃CN, and CHCl₃). This outcome may be based on the better solubility of

TABLE 5 Effect of solvents in synthesis of polysubstituted pyrrole **5a**

Solvent ^a	Time (min)	Yield (%) ^b
DCM	60	43
DMF	60	48
THF	60	54
CH ₃ CN	60	53
CHCl ₃	60	55
MeOH	30	78
AcOH	30	76
EtOH	15	92
H ₂ O	15	88
H ₂ O/EtOH	10	98

^aReaction conditions; **5a**, **1a** (1 mmol), **2** (1.5 mmol), **3** (1 mmol), **4** (1 mmol), and catalyst (0.1 mmol) in mixture of water and ethanol (3:1 ratio) by ultrasonic irradiation condition, 10 min.

^bIsolated yields based on **5a**.

TABLE 4 Amounts of HYHPd catalyst used in synthesis of polysubstituted pyrroles (**5a–o**)

TABLE 6 Use of different Lewis acid and Lewis base by ultrasonic (US) irradiation for reaction **5a**^a

Entry	Cat (mol%)	Conditions ^a	Yield (%) ^b
1	No catalyst, No US	Water/ethanol, 1 day	Trace
2	No catalyst	Water/ethanol, 1 hr	56
3	AlCl ₃ (10)	Water/ethanol, 10 min	47
4	MgCl ₂ (10)	Water/ethanol, 10 min	44
5	FeCl ₃ ·6H ₂ O (10)	Water/ethanol, 10 min	58
6	Fe (OTf) ₃ (10)	Water/ethanol, 10 min	71
7	(10)ZnBr ₂	Water/ethanol, 10 min	72
8	CuCl ₂ (10)	Water/ethanol, 10 min	65
9	PdCl ₂ (10)	Water/ethanol, 10 min	88
10	Pd (OAc) ₂ (10)	Water/ethanol, 10 min	86
11	<i>p</i> -TsOH (10)	Water/ethanol, 10 min	76
12	Et ₃ N(10)	Water/ethanol, 10 min	67
13	TBABr ^[c] (10)	Water/ethanol, 10 min	64
14	TiCl ₄ (10)	Water/ethanol, 10 min	69
15	HYHCu (10)	Water/ethanol, 10 min	83
16	HYHFe (10)	Water/ethanol, 10 min	91
17	HYHPd (10)	Water/ethanol, 10 min	98
18	HYHPd (10) No US	Water/ethanol, 10 min	88

Note: The row in bold explains the best one of condition reaction and amount of catalyst.

^aReaction conditions: **1a** (1 mmol), **2** (1.5 mmol), **3** (1 mmol), **4** (1 mmol) and Catalyst (10% mol) in mixture of water and ethanol (3:1 ratio) by ultrasonic condition, 10 min.

^bIsolated yields based on **5a**.

^cTetrabutylammonium bromide, US (ultrasonic).

reactants in polar solvents. Also, it is obvious that the reaction conducted under a mixture of solvents (water/ethanol; v/v; 3/1) is the best choice for the synthesis of polysubstituted pyrrole **5a**. We preferred this mixture because is environmentally friendly, safe and cheap in comparing with organic solvents.

3.8.3 | Comparative study with other Lewis acid and Lewis base catalysts

In recent years, palladium (II) complexes have received considerable attention as a mild Lewis acid catalyst for an array of organic transformations. The reaction of benzaldehyde **1**, aniline **2**, acetylacetone **3**, and nitromethane **4** was adjusted at the same conditions (Table 6) but under variable catalysts. Various types of Lewis acids and Lewis base such as AlCl₃, MgCl₂, PdCl₂, Pd (OAc)₂, FeCl₃·6H₂O, Fe (OTf)₃, ZnBr₂, CuCl₂, TiCl₄, *p*-TsOH, Et₃N, and TBABr^c were tested at optimum conditions (reported in the previous part). When tested HYHCu, HYHFe, HYHPd (subjected to ultrasonic), and HYHPd (not subjected to ultrasonic) (Table 6, Entries 15–18), HYHPd that subjected to ultrasonic was the most

effective catalyst and afforded desired product **5a** in 98% yield (Table 6, Entry 17).

As can be seen in Table 7, the catalytic activity of HYHPd was compared with diverse catalysts such as which have been previously employed as catalysts in our model reaction. In terms of the yield of the products, the present work exhibited the perfect efficiency than the other promoters.

3.8.4 | Recycling of HYHPd catalyst

The green and economic aspects of this synthetic protocol were further studied by examining the possibility of recovery for HYHPd catalyst, for reusing in the next runs of synthesis. Progressive reaction model with four reactants (benzaldehyde **1**, aniline **2**, acetylacetone **3**, and nitromethane **4** (water/ethanol (3:1 ratio), refluxed 15 min) was repeated five times in presence of HYHPd to synthesize **5a**. Therefore, inevitable loss of catalyst during the recovery process was expected. Trials done for HYHPd recovery were graphed (Figure 7) and exhibited reuse of HYHPd for five consecutive cycles without significant loss of catalytic activity. But when we tried next

Entry catalyst	Catalyst amount	Yield (%)	Reference
FeCl ₃	10 mol.%	56	Konkala et al. ^[20a]
β -cyclodextrin	10 mol.%	90	Rostamnia et al. ^[20b]
2-Hydroxy propyl-b-cyclodextrin	10 mol.%	29	Rostamnia et al. ^[20b]
Methyl- β -cyclodextrin	10 mol.%	30	Rostamnia et al. ^[20b]
Sodium dodecyl sulfate	10 mol.%	20	Rostamnia et al. ^[20b]
Fe (OTf) ₃	10 mol.%	38	Konkala et al. ^[20a]
PEG-400	10 mol.%	Trace	Rostamnia et al. ^[20b]
HYHPd	10 mol.%	98	Present work

TABLE 7 The comparison of the catalytic activity of HYHPd with formerly reported catalysts

Note: The row in bold explains the best one of condition reaction and amount of catalyst.

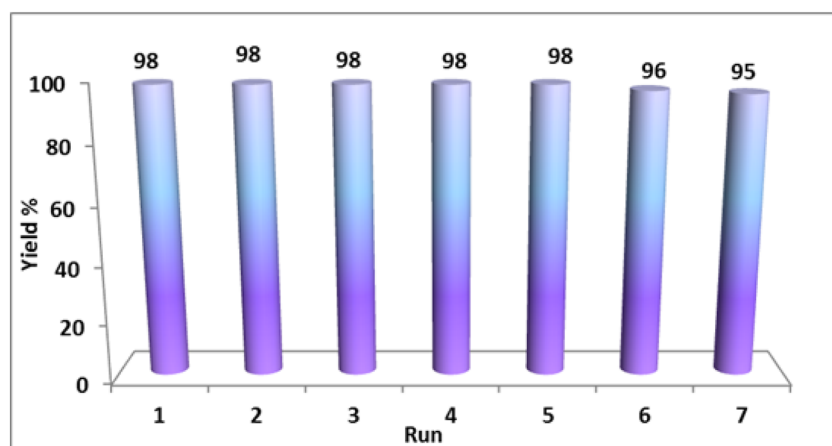


FIGURE 7 Recyclability of HYHPd in the model reaction

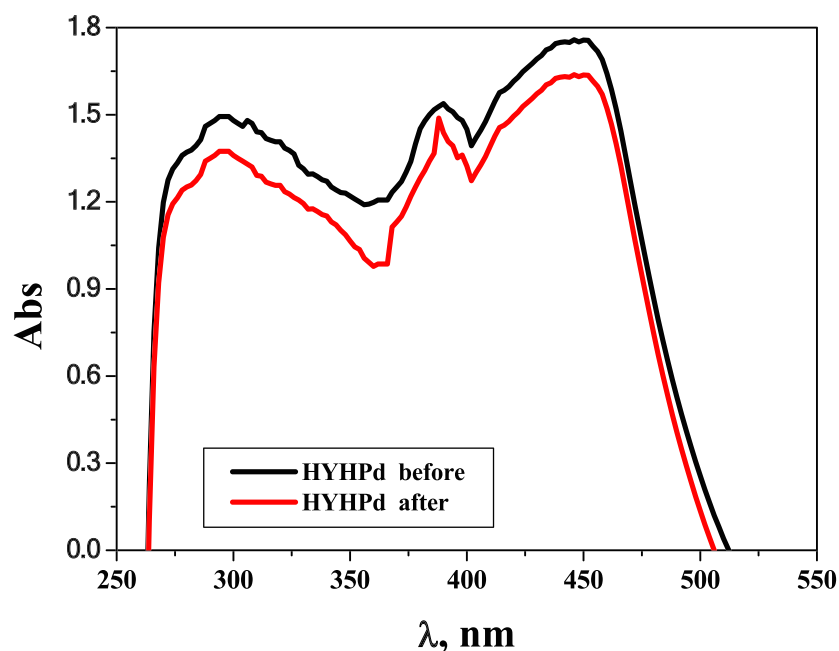
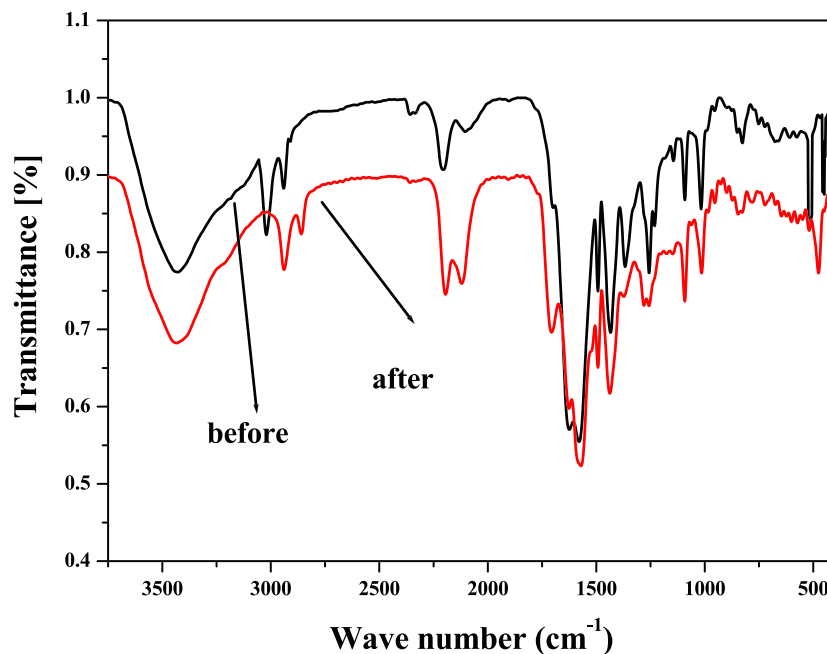


FIGURE 8 Molecular electronic spectra of HYHPd catalyst before and after the investigated catalytic reaction

runs (6 and 7), low catalytic activity was observed under the same conditions. Molecular electronic and IR spectra for the investigated HYHPd catalyst before and catalytic

reaction are presented in Figures 8 and 9. It was noted that there is no notable change in the spectra of the investigated HYHPd catalyst after its recycling from

FIGURE 9 Infrared (IR) spectra of HYHPd catalyst before and after the investigated catalytic reaction



the reaction medium. Also, the elemental analyses for HYHPd catalyst (C [40.58%], H [4.91%], and N [8.72%]) after the recycling of catalyst were in a good agreement with analyses before the reaction.

3.8.5 | Plausible mechanism for catalytic pathway

We proposed the most acceptable mechanism for the synthetic protocol (Scheme 3) by which pyrroles can be obtained from nitro alkenes and β -enamino ketones or esters through cyclization.^[53] Nitroalkenes can be prepared from aldehyde, nitroalkane, and β -enamino ketones or esters via reaction of the 1,3-dicarbonyl compound with amines catalyzed by Pd (II) ions (Scheme 3).^[54–56] Large surface area and pore size of HYHPd complex allow organic substrates to access Pd (II) ions in the crystal structure. Also, highly dispersed Pd (II) in HYHPd complex, which has free coordination position (z axis), makes Pd (II) ions as highly active sites promote 4CRs. On the other hand, the coordination between ligands and Pd (II) ions could keep physical and chemical stability for Pd (II) ions in the complex during the catalytic procedure. Therefore, the construction of pyrrole ring via Michael reaction of β -enamino ketones or esters and nitroalkenes could be achieved in presence of HYHPd catalyst. Excellent catalytic activity role can be realized for 4CRs.

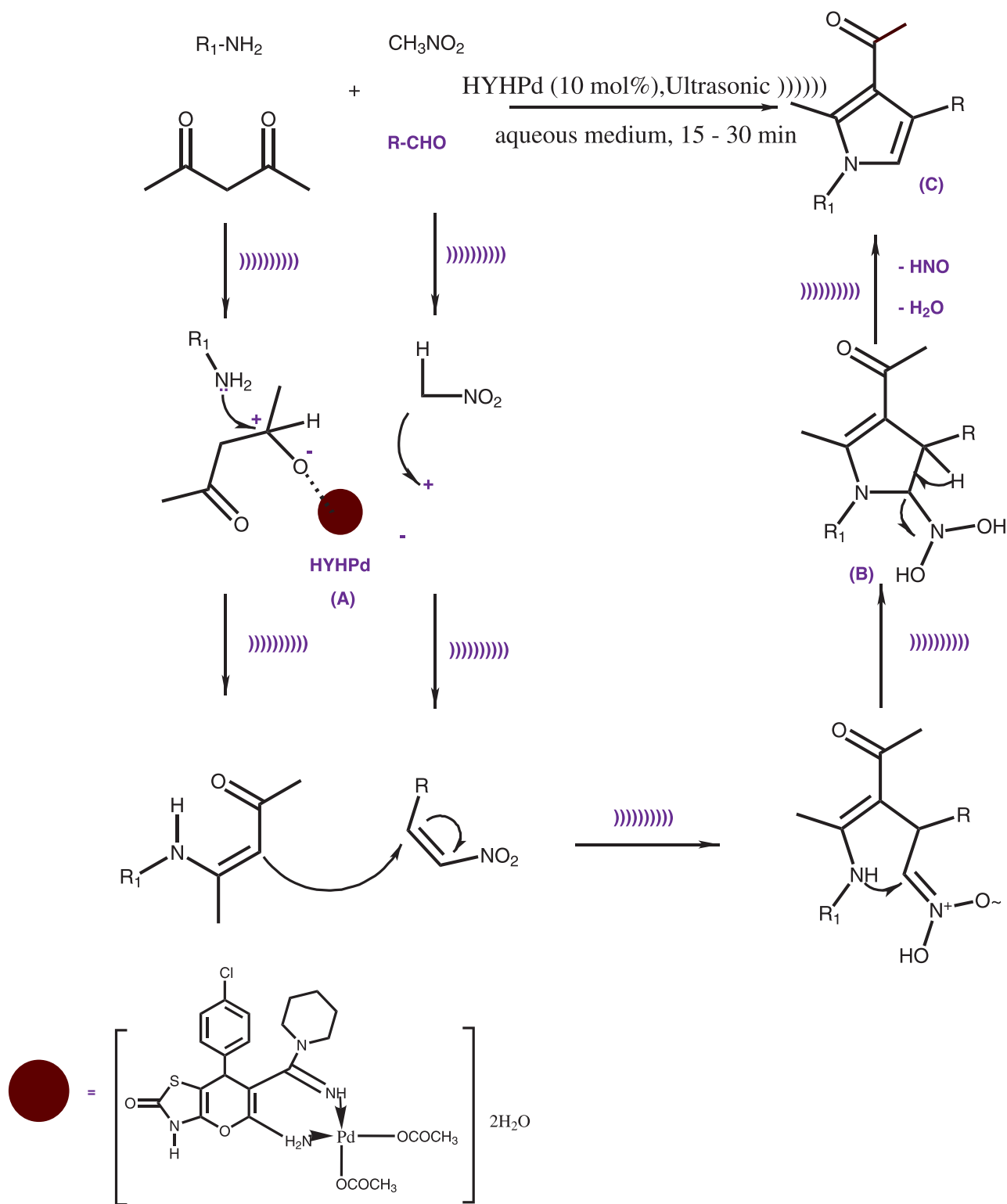
In conclusion, we successfully developed a facile and efficient method for synthesis of different polysubstituted pyrroles derivatives from the reaction of aromatic

aldehyde **1**, aromatic amine **2**, acetylacetone **3**, and nitromethane **4** in presence of HYHPd catalyst subjected to ultrasonic at mild conditions. As known, ultrasound has long been used to create small, uniform crystals through behavior discussed by several hypotheses.^[57] Consequently, the superior catalysis function of HYHPd complex that subjected to ultrasonic may refer to the influence of ultrasound vibrations on the order of particles inside the crystal, which may improve its catalytic role.

The catalytic path of HYHPd in the four-component reaction that ended by aromatization of polysubstituted pyrroles derivatives was conducted in environmentally benign conditions. The advantages of HYHPd and US were summarized to afford precipitates from the multicomponent system in water/ethanol to enhance aromatization of polysubstituted pyrroles. The higher catalytic activity of it is ascribed to its high acidity and water tolerance. Also, the superiority of using HYHPd in the synthesis of polysubstituted pyrroles in comparison to other Lewis acids is based on the mildness of conversion and compatibility with various functional groups, which makes this procedure attractive to synthesize other various derivatives.

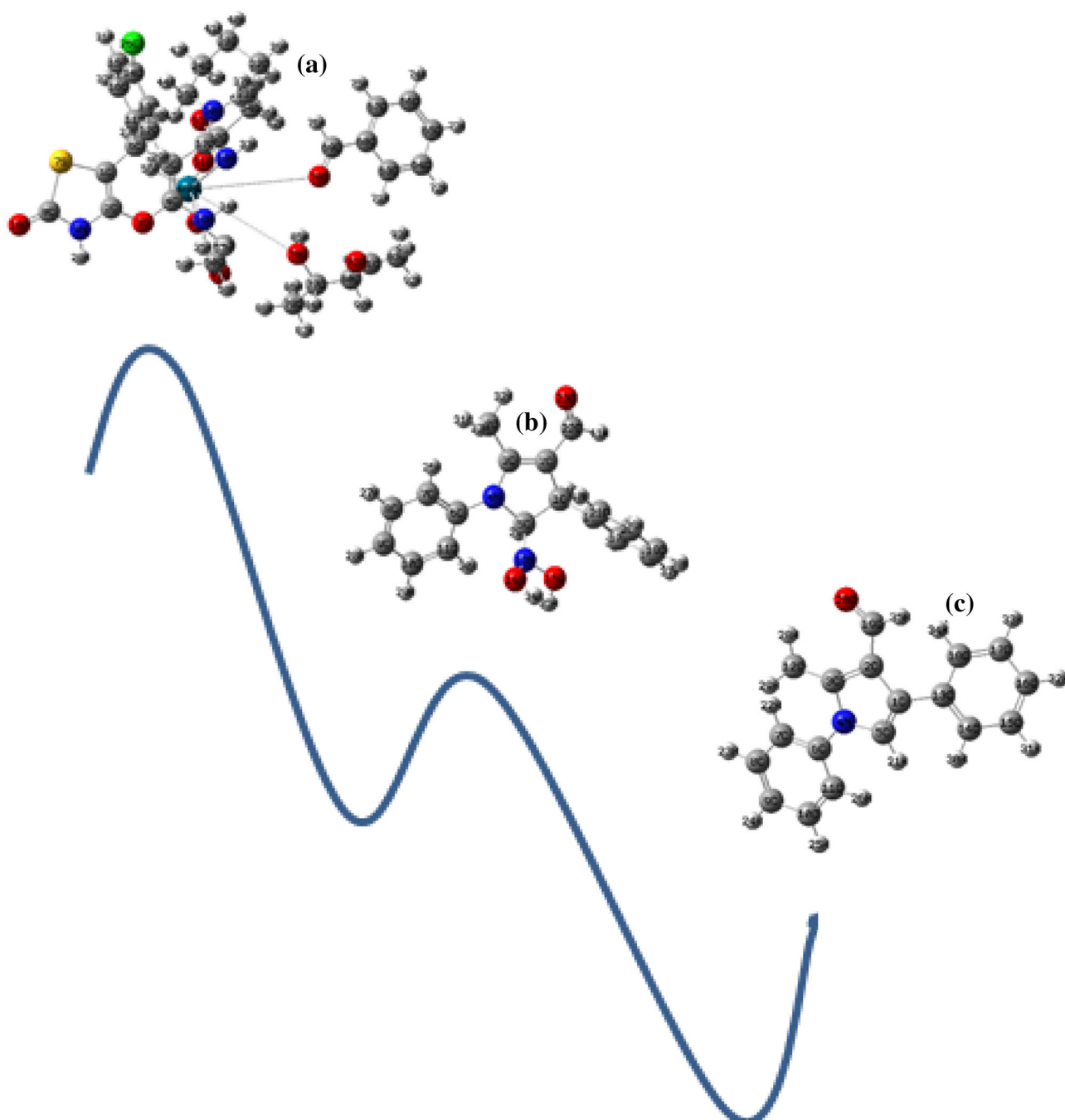
3.8.6 | Theoretical bases for suggested mechanism

Interestingly, on the basis of the following remarks, we could summarize the promising properties of HYHPd complex versus catalytic:



SCHEME 3 Suggested mechanism for synthesis of polysubstituted pyrrole derivatives and the catalytic role of HYHPd

1. First, for its differentiating catalytic behavior, the square planar geometry of the complex is considered to be a successful supporter. This is due to the presence of two empty z axis sites capable of interaction and forming five or six coordinations in the
2. intermediate state (A) without the need to substitute any secondary ligand.
2. The crystal properties of the HYHPd complex showed a large surface area of the complex, which in general is favorable for catalysis. Oxygen atoms also have an



SCHEME 4 Free-energy profile for the catalytic pathway

important contribution to interaction with other surfaces; oxygen could start trapping the compounds over the surface, which was considered to be the first step in any catalytic activity within the medium of reaction.

- Moreover, the lower energy gap (ΔE) value with Pd (II) complex indicates the overlapping between the valence band and conduction band also the electrons in the outer shell are labial and easily excited. This is a preferable feature in catalysis due to the lower activation energy needed in the intermediate step.

Moreover, the intermediate compounds **A**, **B**, and **C** that were suggested during the synthesis process of polysubstituted pyrrole derivatives (Scheme 3) in presence of HYHPd catalyst were optimized to evaluate their stability level. This optimization was carried out under DFT/B3LYP method and valence double-zeta polarizable basis set (6-31G*). The recorded free energy of these intermediates (**A**, **B**, and **C**) were E (a. u.), -1673.9621 , -1031.3635 , and -820.2661 , respectively. This indicates the relative lower stability of intermediate **A**, which

presented the interaction of the complex with the reactants. The presence of reactants around Pd (II) as a central atom may facilitate the formation of other intermediates as **B**, which appeared fairly stable (−1031.3635 a.u.), while the product (**C**) exhibited a high stability (−820.2661 a. u.) in comparison to the former intermediates. The suggested free-energy profile was schematically drawn (Scheme 4), for clarification.

4 | CONCLUSION

New Fe (III), Cu (II), and Pd (II) complexes were prepared from new thiazole derivative. These complexes were deliberately characterized by all possible analytical, spectral, and theoretical techniques. After that, their chemical formulae were verified. The spectral data confirm a neutral bi-dentate mode of bonding in all complexes. The complexes were suggested in octahedral geometry except Pd (II) complex is in a square planar configuration. The conformational analysis and contact efficiency inside crystal packing of complexes offer important physical characteristics that discriminate the Pd (II) complex over the other two. The use of Pd (II) complex in the hetero-catalytic process is the main application aimed in this study. The complex revealed distinguish catalytic behavior in one-put synthesis for polysubstituted pyrroles derivatives using ultrasonic irradiation. Its success was controlled by using mild conditions in the green strategy. The targeted products were obtained in a short time with high yield and the catalyst was recovered easily and reused many times till five times by the same efficiency. The mechanism of the catalytic process was suggested and supported by theoretical bases.

ACKNOWLEDGMENT

Dr. Mohamed acknowledges Taif University Researchers Supporting Project number (TURSP-2020/43), Taif University, Taif, Saudi Arabia.

AUTHOR CONTRIBUTIONS

Mahmoud Abd El Aleem Ali Ali El-Remaily: Supervision. **Nashwa M. El-Metwaly:** Supervision. **Tahani M. Bawazeer:** Project administration. **Mohamed E. Khalifa:** Formal analysis. **tarek El-Dabea:** Methodology. **Ahmed M. Abu-Dief:** Methodology.

DATA AVAILABILITY STATEMENT

The data that support findings of this study are available in the supporting information and the corresponding author upon reasonable request.

ORCID

Mahmoud Abd El Aleem Ali Ali El-Remaily  <https://orcid.org/0000-0002-3591-0077>

Nashwa M. El-Metwaly  <https://orcid.org/0000-0002-0619-6206>

Tahani M. Bawazeer  <https://orcid.org/0000-0003-1294-9988>

Mohamed E. Khalifa  <https://orcid.org/0000-0003-4914-4796>

Tarek El-Dabea  <https://orcid.org/0000-0002-5359-6931>

Ahmed M. Abu-Dief  <https://orcid.org/0000-0003-3771-9011>

REFERENCES

- [1] N. C. Eddingsaas, K. S. Suslick, *Nature* **2006**, *444*, 163.
- [2] N. Ghaffari Khaligh, F. Shirini, *Ultrason. Sonochem.* **2015**, *22*, 397.
- [3] K. S. Suslick, *Sci. Am.* **1989**, *260*, 80.
- [4] S. Allahyari, M. Haghghi, A. Ebad, S. Hosseinzadeh, *Ultrason. Sonochem.* **2014**, *21*, 663.
- [5] a) A. Ramazani, M. Rouhani, S. W. Joo, *Ultrason. Sonochem.* **2016**, *28*, 393; b) H. Xu, B. W. Zeiger, K. S. Suslick, *Chem. Soc. Rev.* **2013**, *42*, 2555.
- [6] a) R. A. Jones, G. P. Bean, *The Chemistry of Pyrroles*, Academic Press, London **1977** 1; b) R. J. Sundberg, in *Comprehensive Heterocyclic Chemistry*, (Eds: A. R. Katritzky, C. W. Rees) Vol. 4, Pergamon Press, Oxford **1984** 370.
- [7] a) M. A. A. El-Remaily, O. M. Elhady, *Appl. Organometal. Chem.* **2019**, *33*, 4989; b) M. A. A. El-Remaily, O. M. Elhady, *Tetrahedron Lett.* **2016**, *57*, 435; c) M. A. A. El-Remaily, H. A. Hamad, *J. Mol. Cata. A: Chem.* **2015**, *404*, 148; d) M. A. A. El-Remaily, A. M. Abu-Dief, *Tetrahedron* **2015**, *71*, 2579; e) M. A. A. El-Remaily, *Tetrahedron* **2014**, *70*, 2971; f) M. A. A. El-Remaily, *Chin. J. Cata* **2015**, *36*, 1124; g) A. M. M. Soliman, S. K. Mohamed, M. A. A. El-Remaily, H. Abdel-Ghany, *Eur. J. Med. Chem.* **2012**, *47*, 138; h) M. A. A. El-Remaily, S. K. Mohamed, *Tetrahedron* **2014**, *70*, 270; i) M. A. A. El-Remaily, A. M. M. Soliman, *J. Sulfur Chem.* **2016**, *37*, 70; j) S. Ni, M. A. A. El-Remaily, J. Franzén, *Adv. Synth. Catal.* **2018**, *360*, 4197.
- [8] a) M. A. A. El-Remaily, A. M. Abu-Dief, O. M. Elhady, *Appl. Organometal. Chem.* **2019**, *33*, 5005; b) M. A. A. El-Remaily, A. M. Abu-Dief, M. R. El-Khatib, *Appl. Organometal. Chem.* **2016**, *30*, 1022; c) M. A. A. El-Remaily, A. M. M. Soliman, O. M. Elhady, *ACS Omega* **2020**, *5*, 6194; d) E. A. Ahmed, A. M. M. Soliman, A. M. Ali, M. A. A. El-Remaily, *Appl. Organometal. Chem.* **2021**, *35*, e6197; e) M. A. A. El-Remaily, O. M. Elhady, *ChemistrySelect* **2020**, *5*(39), 12098; f) M. A. A. El-Remaily, H. A. Hamad, A. Soliman, O. M. Elhady, *Appl. Organometal. Chem.* **2021**, *35*, e6238; g) E. K. Shokr, M. S. Kamel, H. Abdel-Ghany, M. A. A. El-Remaily, *Curr. Res. Green Sustain. Chem.* **2021**, *4*, 100090; h) H. A. Hamad, H. Nageh, H. M. El-Bery, A. Kasry, F. Carrasco-Marín, O. M. Elhady, A. M. M. Soliman, M. A. A. El-Remaily, *J. Colloid Interface Sci.* **2021**, *599*, 227; i) E. K. Shokr, M. S. Kamel, H. Abdel-Ghany, M. A. A. El-Remaily, *Optik* **2021**, *243*, 167385.

- [9] a) M. Biava, R. Fioravanti, G. C. Porretta, D. Deidda, C. Maullo, P. Pompei, *Bioorg. Med. Chem. Lett.* **1999**, *9*, 2983; b) P. Cozzi, N. Mongelli, *Curr. Pharm. Des.* **1998**, *4*, 181; c) S. Yamaguchi, K. J. Tamao, *Organomet. Chem.* **2002**, *653*, 223; d) S. Rostamnia, H. G. Hossieni, E. Doustkhah, *J. Organomet. Chem.* **2015**, *791*, 18.
- [10] a) J. Chen, H. Wu, Z. Zheng, C. Jin, X. Zhang, W. Su, *Tetrahedron Lett.* **2006**, *47*, 5383; b) A. Alizadeh, S. Rostamnia, L. G. Zhu, *Tetrahedron Lett.* **2010**, *51*(36), 4750; c) S. Rostamnia, T. Rahmani, *Appl. Organomet. Chem.* **2015**, *29*(7), 471.
- [11] a) C. V. Galliford, K. A. Scheidt, *J. Org. Chem.* **2007**, *72*, 1811; b) F. Ragaini, S. Cenini, D. Brignoli, M. Gasperini, E. Gallo, *J. Org. Chem.* **2003**, *68*, 460.
- [12] a) J.-Y. Wang, X.-P. Wang, Z.-S. Yu, W. Yu, *Adv. Synth. Catal.* **2009**, *351*, 2063; b) P. Mondal, S. Chatterjee, K. Nurjamal, S. Maity, A. Bhaumik, G. Brahmachari, P. Ghosh, C. Mukhopadhyay, *Catal. Commun.* **2020**, *139*, 105966.
- [13] R.-L. Yan, J. Luo, C.-X. Wang, C.-W. Ma, G.-S. Huang, Y.-M. Liang, *J. Org. Chem.* **2010**, *75*, 5395.
- [14] Q. Li, A. Fan, Z. Lu, Y. Cui, W. Lin, Y. Jia, *Org. Lett.* **2010**, *12*, 4066.
- [15] a) S. Chiba, Y.-F. Wang, G. Lapointe, K. Narasaka, *Org. Lett.* **2008**, *10*, 313; b) A. Ahadi, H. Alamgholiloo, S. Rostamnia, X. Liu, M. Shokouhimehr, D. A. Alonso, & R. Luque, **2019**, *11*, 4803. <https://doi.org/10.1002/cctc.201900486>
- [16] N. D. Smith, D. Huang, N. D. P. Cosford, *Org. Lett.* **2002**, *4*, 3537.
- [17] a) X.-T. Liu, L. Hao, M. Lin, L. Chen, Z.-P. Zhan, *Org. Biomol. Chem.* **2010**, *8*, 3064; b) S. Rana, M. Brown, A. Dutta, A. Bhaumik, C. Mukhopadhyay, *Tetrahedron Lett.* **2013**, *54*(11), 1371.
- [18] a) S. Ngwerume, J. E. Camp, *J. Org. Chem.* **2010**, *75*, 6271; b) S. Rostamnia, A. Morsali, *Inorg. Chim. Acta* **2014**, *411*, 113; c) S. Rostamnia, E. Doustkhah, *Tetrahedron Lett.* **2014**, *55*(15), 2508.
- [19] a) Y. Wang, X. Bi, D. Li, P. Liao, Y. Wang, J. Yang, Q. Zhang, Q. Liu, *Chem. Commun.* **2011**, *47*, 809; b) S. Rostamnia, H. Alamgholiloo, M. Jafari, *Appl. Organomet. Chem.* **2018**, *32*(8), e4370.
- [20] a) K. Konkala, R. Chowrasia, P. S. Manjari, N. L. C. Domingues, R. Katla, *RSC Adv.* **2016**, *6*, 43339; b) S. Rostamnia, X. Liu, D. Zheng, *J. Colloid Interface Sci.* **2014**, *432*, 86; c) H. Alamgholiloo, S. Rostamnia, A. Hassankhani, X. Liu, A. Eftekhari, A. Hasanzadeh, M. Shokouhimehr, *J. Colloid Interface Sci.* **2020**, *567*, 126; d) S. Rostamnia, E. Doustkhah, *J. Magn. Magn. Mater.* **2015**, *386*, 111; e) A. Alizadeh, N. Zohreh, S. Rostamnia, *Tetrahedron* **2007**, *63*(34), 8083.
- [21] A. M. Abu-Dief, N. M. El-Metwaly, S. O. Alzahrani, F. Alkhatib, H. M. Abumelha, T. El-Dabea, M. A. A. El-Remaily, *Res. Chem. Intermed.* **2021**, *47*, 1979.
- [22] a) A. W. Coats, J. P. Redfern, *Nature* **1964**, *201*, 68; b) L. H. Abdel-Rahman, A. M. Abu-Dief, F. M. Atlam, A. A. H. Abdel-Mawgoud, A. A. Alothman, A. M. Alsalmeh, A. Nafady, *J. Coord. Chem.* **2020**, *73*(23), 3150; c) A. M. Abu-Dief, L. H. Abdel-Rahman, A. A. Abdelhamid, A. A. Marzouk, M. R. Shehata, M. A. Bakheet, O. A. Almaghrabi, A. Nafady, *Spectrochim. Acta a* **2020**, *228*, 117700.
- [23] a) T. Taakeyama, F. X. Quinn, *Thermal Analysis Fundamentals and Applications to Polymer Science*, John Wiley and Sons, Chichester **1994**; b) L. H. Abdel-Rahman, A. M. Abu-Dief, H. Moustafa, A. A. H. Abdel-Mawgoud, *Arabian J. Chem.* **2020**, *31*(1), 649; c) A. M. Abu-Dief, N. M. El-Metwaly, S. O. Alzahrani, F. Alkhatib, M. M. Abualnaja, T. El-Dabea, M. A. A. El-Remaily, *J. Mol. Liq.* **2021**, *326*, 115277.
- [24] a) H. M. Abd El-Lateef, A. M. Abu-Dief, M. A. A. Mohamed, *J. Mol. Struct.* **2017**, *1130*, 522; b) H. M. Abd El-Lateef, A. M. Abu-Dief, B. E. D. M. El-Gendy, *J. Electroanal. Chem.* **2015**, *758*, 135.
- [25] a) L. H. Abdel-Rahman, A. M. Abu-Dief, M. R. Shehata, F. M. Atlam, A. A. H. Abdel-Mawgoud, *Appl. Organomet. Chem.* **2019**, *33*, e4699; b) L. H. Abdel-Rahman, A. M. Abu-Dief, S. K. Hamdan, A. A. Seleem, *Int. J. Nano. Chim.* **2015**, *1*, 65; c) L. H. Abdel-Rahman, A. M. Abu-Dief, M. S. S. Adam, S. K. Hamdan, *Catal. Lett.* **2016**, *146*, 1373; d) A. M. Abu-Dief, L. H. Abdel-Rahman, A. A. H. Abdel-Mawgoud, *Appl Organometal Chem.* **2020**, *34*(2), e5373.
- [26] a) L. H. Abdel-Rahman, A. M. Abu-Dief, M. Ismael, M. A. A. Mohamed, N. A. Hashem, *J. Mol. Struct.* **2016**, *1103*, 232; b) A. M. Abu-Dief, H. M. El-Sagher, M. R. Shehata, *Appl. Organometal Chem.* **2019**, *33*, e4943.
- [27] a) L. H. Abdel-Rahman, A. M. Abu-Dief, E. F. Newair, S. K. Hamdan, *J. Photochem. Photobiol. B* **2016**, *160*; b) L. H. Abdel-Rahman, A. M. Abu-Dief, H. Mostafa, S. K. Hamdan, *Appl. Organometal. Chem.* **2017**, *31*, e3555; c) L. H. Abdel-Rahman, A. M. Abu-Dief, R. M. El-Khatib, S. M. Abdel-Fatah, *Bioorg. Chem.* **69**(2016), 140.
- [28] a) Modeling and Simulation Solutions for Chemicals and Materials Research, Materials Studio (Version 5.0), Accelrys software Inc., San Diego, USA. Available online at: www.accelrys.com **2009**; b) H. Katouah, A. Sayqal, A. M. Al-Solimy, H. M. Abumelha, R. Shah, F. Alkhatib, S. Alzahrani, R. Zaky, N. M. El-Metwaly, *J. Mol. Liq.* **2020**, *320*, 114380; c) R. Shah, H. Katouah, A. A. Sedayo, M. Abualnaja, M. M. Aljohani, F. Saad, R. Zaky, N. M. El-Metwaly, *J. Mol. Liq.* **2020**, *319*, 114116; d) S. Alzahrani, M. Morad, A. Bayazeed, M. M. Aljohani, F. Alkhatib, R. Shah, H. Katouah, H. M. Abumelha, I. Althagafi, R. Zaky, N. M. El-Metwaly, *J. Mol. Struct.* **2020**, *1218*, 128473.
- [29] M. J. Frisch, G. W. Trucks, J. A. Pople, *Gaussian 09, Revision B.2*, Gaussian, Inc., Pittsburgh, PA **2009**.
- [30] W. J. Hehre, L. Radom, P. V. R. Schlyer, J. A. Pople, *Ab Initio Molecular Orbital Theory*, Wiley, New York **1986**.
- [31] A. Kessi, B. Delley, *Int. J. Quantum Chem.* **1998**, *68*, 135.
- [32] K. M. P. Kumar, B. C. V. Kumar, P. R. Kumar, R. J. Butcher, H. K. Vivek, P. A. Suchetan, H. D. Revanasiddappa, S. Foro, *Appl Organometal Chem.* **2020**, e5634.
- [33] K. Nakamoto, *Infrared and Raman Spectra of Inorganic and Coordination Compounds: Part B: Applications in Coordination, Organometallic, and Bioinorganic Chemistry*, John Wiley & Sons Inc., Hoboken, NJ **2009**.
- [34] S. S. Jawoor, S. A. Patil, S. S. Toragalmath, *J. Coord. Chem.* **2018**, *71*(2), 271.
- [35] A. S. Munde, A. N. Jagdale, S. M. Jadhav, T. K. Chondhekar, *J. Serb. Chem. Soc.* **2010**, *75*, 349.
- [36] R. A. Kusanur, M. Ghate, M. V. Kulkarni, *J. Chem. Sci.* **2004**, *116*, 265.
- [37] F. E. Mabbs, D. J. Machin, *Magnetism and Transition Metal Chemistry*, Chapman and Hall, London **1973**.

- [38] a) A. B. Getsoian, Z. Zhai, A. Bell, *J. Am. Chem. Soc.* **2014**, 136(39); b) N. F. Mott, E. A. Davis, *Electrochemical Process in Non-crystalline Materials*, Calendron Press, Oxford **1979**.
- [39] F. Karipcin, B. Dede, Y. Caglar, D. Hur, S. Ilcan, M. Caglar, Y. Sahin, *Optic Commun.* **2007**, 272, 131.
- [40] A. N. M. A. Alaghaz, M. E. Zayed, S. A. Alharbi, R. A. A. Ammar, *J. Mol. Struct.* **2015**, 1087, 60.
- [41] a) H. A. El-Boreay, S. A. Aly, *Met.-Org. Nano-Met. Chem.* **2013**, 43, 1130; b) H. El-Boraey, F. El-Saied, S. Aly, *J. Therm. Anal. Calorim.* **2008**, 96, 599.
- [42] A. A. S. Al-Hamdani, R. S. A. Al-luhaibi, *Res. J. Pharm, Biolog. Chem. Sci.* **2017**, 8, 164.
- [43] M. Montazerzohori, S. MojahediJahromi, A. Masoudiasl, P. McArdle, *Spectrochim. Acta a* **2015**, 5, 517.
- [44] a) L. H. Abdel-Rahman, A. M. Abu-Dief, M. Basha, A. A. H. Abdel-Mawgoud, *Appl. Organometal Chem.* **2017**, e3750; b) L. H. Abdel-Rahman, M. S. S. Adam, A. M. Abu-Dief, H. Moustafa, M. T. Basha, A. S. Aboraia, B. S. Al-Farhan, H. El-Sayed, *Appl Organometal Chem.* **2018**, e4527.
- [45] D. X. West, J. K. Swearingen, J. Valdés-Martinez, S. Hernández-Ortega, A. K. El-Sawaf, F. V. Meurs, A. Castiñeiras, I. Garcia, E. Bermejo, *Polyhedron* **1999**, 18, 2919.
- [46] F. Alkhatib, A. Hameed, A. Sayqal, A. A. Bayazeed, S. Alzahrani, Z. A. Al-Ahmed, R. Zaky, N. M. El-Metwaly, *Arab. J. Chem.* **2020**, 13(8), 6327.
- [47] L. O. Olasunkanmi, I. B. Obot, E. E. Ebenso, *RSC Adv.* **2016**, 6, 86782.
- [48] Z. El, M. Mcharfi, M. Sfaira, M. Benzakour, A. Benjelloun, M. E. Touhami, *Corros. Sci.* **2013**, 68, 223.
- [49] M. J. Turner, J. J. McKinnon, D. Jayatilaka, M. A. Spackman, *Cryst. Eng. Comm.* **2011**, 13, 1804.
- [50] K. Momma, F. Izumi, *J. Appl. Crystallogr.* **2011**, 44, 1272.
- [51] M. S. Refat, I. Althagafi, N. El-Metwaly, R. Shah, H. Katouah, R. R. Amin, Y. B. Yamany, T. Altalhi, J. Y. Al-Humaidi, *Appl. Organomet. Chem.* **2020**, 34(9), e5766.
- [52] H. Katouah, A. M. Hameed, A. Alharbi, F. Alkhatib, R. Shah, S. Alzahrani, R. Zaky, N. M. El-Metwaly, *ChemistrySelect* **2020**, 5(33), 10256.
- [53] a) S. Maiti, S. Biswas, U. Jana, *J. Org. Chem.* **2010**, 75, 1674; b) E. Doustkhah, S. Rostamnia, H. G. Hossieni, R. Luque, *Chem. Select* **2017**, 2(1), 329.
- [54] H. Eshghi, S. M. Seyedi, E. Safaei, M. Vakili, A. Farhadipour, M. B. Mokhtari, *J. Mol. Catal. A: Chem.* **2012**, 430, 363.
- [55] H. Hebbache, Z. Hank, S. Boutamine, M. Meklati, C. Bruneau, J. L. Renaud, *C. R. Chim.* **2008**, 11, 612.
- [56] J. Tang, M. Yang, M. Yang, J. Wang, W. Dong, G. Wanga, *New J. Chem.* **2015**, 39, 4919.
- [57] S. L. Hem, *Ultrasonics* **1967**, 5(4), 202.

SUPPORTING INFORMATION

Additional supporting information may be found online in the Supporting Information section at the end of this article.

How to cite this article: M. A. E. A. A. El-Remaly, N. M. El-Metwaly, T. M. Bawazeer, M. E. Khalifa, T. El-Dabea, A. M. Abu-Dief, *Appl Organomet Chem* **2021**, e6370. <https://doi.org/10.1002/aoc.6370>